

Journal of Mechanics of Materials and Structures

**TWO-DIMENSIONAL FRETTING CONTACT OF PIEZOELECTRIC MATERIALS
UNDER A RIGID CONDUCTING CYLINDRICAL PUNCH**

Jie Su, Liao-Liang Ke and Yue-Sheng Wang

Volume 11, No. 5

December 2016



TWO-DIMENSIONAL FRETTING CONTACT OF PIEZOELECTRIC MATERIALS UNDER A RIGID CONDUCTING CYLINDRICAL PUNCH

JIE SU, LIAO-LIANG KE AND YUE-SHENG WANG

This paper investigates the fretting contact between a transversely isotropic piezoelectric half-plane and a rigid cylindrical punch in a plane strain state. It is assumed that the punch is a perfect conductor with a constant electric potential within the contact region. Since the fretting contact problem is frictional and history dependent, the two bodies are brought into contact first by a monotonically increasing normal load, and then by a cyclic tangential load, which is less than that necessary to cause complete sliding. It is assumed that the contact region contains an inner stick region and two outer slip regions in which Coulomb's friction law is applied. With the use of the superposition principle and Fourier integral transform technique, the problem is reduced to a set of coupled Cauchy singular integral equations. An iterative method is used to determine the unknown stick/slip region, normal contact pressure, electric charge and tangential traction. The effects of the friction coefficient, electric load and conductivity of the punch on the surface electromechanical fields are discussed during different loading phases.

1. Introduction

Piezoelectric materials are important smart materials and have been widely used in various electromechanical devices such as actuators, sensors, transducers and micropower generators. Piezoelectric devices are often subjected to highly localized loading indented by a concentration load or rigid punches. Thus, failure and degradation of the piezoelectric components may be caused by the inharmonious contact between piezoelectric devices and the punch due to the innate brittleness of the piezoelectric ceramics. As a result of the aforementioned reasons, many theoretical investigations concerning indentation, frictionless contact and frictional contact of piezoelectric materials have received considerable concerns and been solved perfectly.

Using the state space framework, Sosa and Castro [1994] obtained the solutions of a piezoelectric half-plane loaded by a concentrated line force and a concentrated line charge. Fan et al. [1996] investigated the two-dimensional contact problem of an anisotropic piezoelectric half-plane by the nonslip or slip indenter. Chen [1999] analyzed the contact problem of an inclined rigid conducting circular flat punch indenting a transversely isotropic piezoelectric half-space. Ding et al. [2000] investigated the three-dimensional frictionless contact problem including a spherical indenter, a conical indenter and an upright circular flat indenter on a transversely isotropic piezoelectric half-space. The contact problem of piezoelectric materials was also examined by Giannakopoulos and Suresh [1999], Chen [2000], Ramirez and Heyliger [2003], Wang et al. [2008], Zhou and Lee [2012] and Wu et al. [2012] for the frictionless case; Makagon

Liao-Liang Ke is the corresponding author.

Keywords: fretting contact, cyclic load, piezoelectric materials, conducting punch, singular integral equation.

et al. [2009], Zhou and Lee [2011; 2014] and Ma et al. [2014] for the sliding frictional case; and Chen and Yu [2005] and Guo and Jin [2009] for the adhesive case.

Fretting is a frictional contact phenomenon that occurs when two bodies are brought into contact by a normal load, and are subjected to cyclic tangential loads causing small relative oscillations with respect to each other. The whole contact surface is divided into an inner stick region, where there is no relative motion between the two bodies, and two outer slip regions at the two edges. The surface tractions near the ends of contact, where the contact surfaces undergo the relative tangential motion, initiate surface cracks that are known as fretting fatigue. Contact damage and fretting fatigue, which occur in engineering structures, gas turbine engines, electric power, aircraft, traffic tools, etc., are the main causes of failure of key components. In some engineering components, the normal load for contacting bodies often does not vary significantly, whereas the tangential load varies cyclically with time. An initial theoretical investigation of the fretting contact was made by Cattaneo [1938], who extended the Hertz contact theory to include a monotonically increasing tangential force. Subsequently, the fretting contact of elastically similar bodies under tangential loading was considered by Mindlin and Deresiewicz [1953], Mindlin et al. [1951], Ciavarella [1998a; 1998b] and Ciavarella and Hills [1999]. The fretting contact of elastically dissimilar bodies was studied by Spence [1973] for monotonically normal loading, Spence [1986] for monotonically tangential loading, Keer and Farris [1987], Hanson et al. [1989], Nowell et al. [1988] for cyclic tangential loading.

Since piezoelectric devices are often in vibration environments, fretting contact damage inevitably occurs in these devices. Unfortunately, so far the work done on the fretting contact of piezoelectric materials is quite limited despite the importance of their application in smart devices. We only found that Su et al. [2015] analyzed the two-dimensional fretting contact between a transversely isotropic piezoelectric half-plane and a rigid insulating cylindrical punch. This paper further studies the fretting contact of a piezoelectric half-plane under a rigid conducting cylindrical punch with a constant electric potential. It is assumed that the whole contact region contains a centrally located stick region between the two regions of slip in which Coulomb's friction law is applied. The two dissimilar bodies are first acted upon by a monotonically increasing normal load, and then by a cyclic tangential load. The fretting contact problem is reduced to a set of coupled Cauchy singular integral equations which are then solved by using an iterative method. The numerical results highlight the effects of the friction coefficient, electric loading and conductivity of the punch on the normal contact pressure, electric charge, tangential traction, in-plane stress and in-plane electric displacement.

Unlike the insulating punch problem in Su et al. [2015], the conductivity of the punch will lead to electric charge distribution at the contact surface. Moreover, the conducting punch problem is governed by the coupled Cauchy singular integral equations with unknown contact pressure and electric charge, which is more difficult to solve than the insulating punch problem. The present results indicate that the insulation of the punch may lead to the concentration of the tangential traction, which may cause a serious influence on the fretting contact damage.

2. Problem formulation

Figure 1 shows the two-dimensional fretting contact between a transversely isotropic piezoelectric half-plane and an infinitely long rigid conducting cylindrical punch with the radius R in a plane strain state.

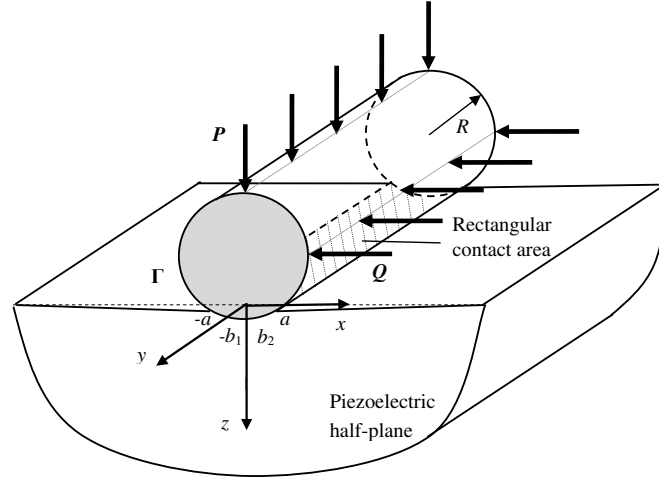


Figure 1. Sketch map of the fretting contact between a homogeneous piezoelectric half-plane and a rigid conducting cylindrical punch in a plane strain state.

The x -axis is along the longitudinal direction at the contact surface while the z -axis is along the thickness direction and points downwards. The two bodies are brought into contact first by a monotonically increasing normal load P to form a contact region $-a \leq x \leq a$, and then by a cyclic tangential load Q which is less than that necessary to cause complete sliding, i.e., $|Q| < \eta P$ where η is the friction coefficient. It is assumed that the punch is a perfect conductor with a constant electric potential ϕ_0 within the contact region. The resultant electric charge Γ is also applied on the punch. The normal displacement component is known from the given punch profile within the contact region whereas the surface normal and tangential tractions are zero outside the contact region.

To solve the present fretting contact problem, the first step is to derive the fundamental solutions of the piezoelectric half-plane subjected to a normal linear load P , a tangential linear load Q and a linear electric charge Γ . Recently, Ma et al. [2014] developed these fundamental solutions which are written as (refer to [Ma et al. 2014, Equations (27)–(29)])

$$u_{x0} = -\frac{if_{11}P}{\pi} \int_0^{+\infty} \frac{\sin(sx)}{s} ds - \frac{f_{12}Q}{\pi} \int_0^{+\infty} \frac{\cos(sx)}{s} ds - \frac{if_{13}\Gamma}{\pi} \int_0^{+\infty} \frac{\sin(sx)}{s} ds, \quad (1)$$

$$u_{z0} = -\frac{f_{21}P}{\pi} \int_0^{+\infty} \frac{\cos(sx)}{s} ds - \frac{if_{22}Q}{\pi} \int_0^{+\infty} \frac{\sin(sx)}{s} ds - \frac{f_{23}\Gamma}{\pi} \int_0^{+\infty} \frac{\cos(sx)}{s} ds, \quad (2)$$

$$\phi_0 = -\frac{f_{31}P}{\pi} \int_0^{+\infty} \frac{\cos(sx)}{s} ds - \frac{if_{32}Q}{\pi} \int_0^{+\infty} \frac{\sin(sx)}{s} ds - \frac{f_{33}\Gamma}{\pi} \int_0^{+\infty} \frac{\cos(sx)}{s} ds. \quad (3)$$

Here $u_{x0} = u_x(x, 0)$ and $u_{z0} = u_z(x, 0)$ are the surface displacement components in the x - and z - directions, respectively; $\phi_0 = \phi(x, 0)$ is the surface electric potential of the piezoelectric half-plane; $i = \sqrt{-1}$ and s is the transform variable; f_{ij} ($i, j = 1, 2, 3$) are the parameters given in the Appendix.

Let $p(x)$, $q(x)$ and $g(x)$ be the normal contact pressure, tangential traction and electric charge within the contact region, respectively. The superposition principle gives the surface displacement components

and surface electric potential

$$u_{x0} = -\frac{if_{11}}{\pi} \int_{-a}^a p(t) \int_0^{+\infty} \frac{\sin[s(x-t)]}{s} ds dt - \frac{f_{12}}{\pi} \int_{-a}^a q(t) \int_0^{+\infty} \frac{\cos[s(x-t)]}{s} ds dt - \frac{if_{13}}{\pi} \int_{-a}^a g(t) \int_0^{+\infty} \frac{\sin[s(x-t)]}{s} ds dt, \quad (4)$$

$$u_{z0} = -\frac{f_{21}}{\pi} \int_{-a}^a p(t) \int_0^{+\infty} \frac{\cos[s(x-t)]}{s} ds dt - \frac{if_{22}}{\pi} \int_{-a}^a q(t) \int_0^{+\infty} \frac{\sin[s(x-t)]}{s} ds dt - \frac{f_{23}}{\pi} \int_{-a}^a g(t) \int_0^{+\infty} \frac{\cos[s(x-t)]}{s} ds dt, \quad (5)$$

$$\phi_0 = -\frac{f_{31}}{\pi} \int_{-a}^a p(t) \int_0^{+\infty} \frac{\cos[s(x-t)]}{s} ds dt - \frac{if_{32}}{\pi} \int_{-a}^a q(t) \int_0^{+\infty} \frac{\sin[s(x-t)]}{s} ds dt - \frac{f_{33}}{\pi} \int_{-a}^a g(t) \int_0^{+\infty} \frac{\cos[s(x-t)]}{s} ds dt. \quad (6)$$

Differentiating Equations (4)–(6) with respect to x yields

$$\frac{\partial u_{x0}}{\partial x} = -\frac{if_{11}}{\pi} \int_{-a}^a p(t) \int_0^{+\infty} \cos[s(x-t)] ds dt + \frac{f_{12}}{\pi} \int_{-a}^a q(t) \int_0^{+\infty} \sin[s(x-t)] ds dt - \frac{if_{13}}{\pi} \int_{-a}^a g(t) \int_0^{+\infty} \cos[s(x-t)] ds dt, \quad (7)$$

$$\frac{\partial u_{z0}}{\partial x} = \frac{f_{21}}{\pi} \int_{-a}^a p(t) \int_0^{+\infty} \sin[s(x-t)] ds dt - \frac{if_{22}}{\pi} \int_{-a}^a q(t) \int_0^{+\infty} \cos[s(x-t)] ds dt + \frac{f_{23}}{\pi} \int_{-a}^a g(t) \int_0^{+\infty} \sin[s(x-t)] ds dt, \quad (8)$$

$$\frac{\partial \phi_0}{\partial x} = \frac{f_{31}}{\pi} \int_{-a}^a p(t) \int_0^{+\infty} \sin[s(x-t)] ds dt - \frac{if_{32}}{\pi} \int_{-a}^a q(t) \int_0^{+\infty} \cos[s(x-t)] ds dt + \frac{f_{33}}{\pi} \int_{-a}^a g(t) \int_0^{+\infty} \sin[s(x-t)] ds dt. \quad (9)$$

Using the Fourier representation of generalized functions gives [Gradshteyn and Ryzhik 2000; Choi and Paulino 2008]

$$\int_0^{\infty} \sin[s(x-t)] ds = \frac{1}{x-t}, \quad \int_0^{\infty} \cos[s(x-t)] ds = \pi \delta(x-t), \quad (10)$$

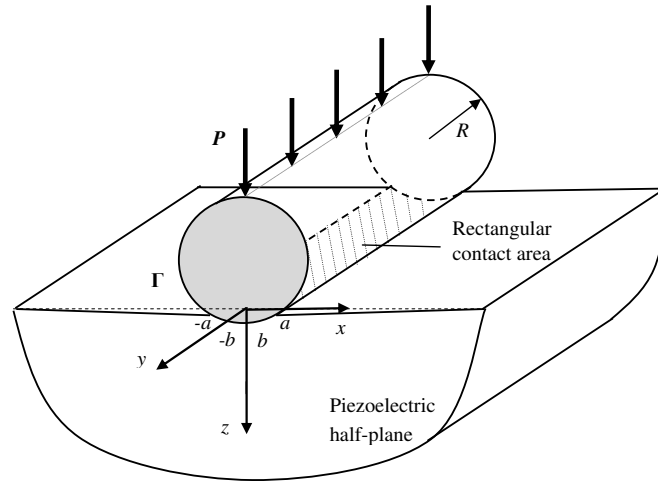


Figure 2. The normal contact with a monotonically increasing normal load P in a plane strain state.

Equations (7)–(9) can be reduced to the following coupled Cauchy singular integral equations for the unknowns $p(x)$, $q(x)$ and $g(x)$

$$-if_{11}p(x) - if_{13}g(x) - \frac{f_{12}}{\pi} \int_{-a}^a \frac{q(t)}{t-x} dt = \frac{\partial u_{x0}}{\partial x}, |x| \leq a, \tag{11}$$

$$-\frac{f_{21}}{\pi} \int_{-a}^a \frac{p(t)}{t-x} dt - if_{22}q(x) - \frac{f_{23}}{\pi} \int_{-a}^a \frac{g(t)}{t-x} dt = \frac{\partial u_{z0}}{\partial x}, |x| \leq a, \tag{12}$$

$$-\frac{f_{31}}{\pi} \int_{-a}^a \frac{p(t)}{t-x} dt - if_{32}q(x) - \frac{f_{33}}{\pi} \int_{-a}^a \frac{g(t)}{t-x} dt = \frac{\partial \phi_0}{\partial x}, |x| \leq a. \tag{13}$$

The resultant force P , Q and resultant electric charge Γ related to $p(x)$, $q(x)$ and $g(x)$ are given by

$$\int_{-a}^a p(t) dt = P, \tag{14}$$

$$\int_{-a}^a q(t) dt = Q, \tag{15}$$

$$\int_{-a}^a g(t) dt = \Gamma. \tag{16}$$

Equations (11)–(16) are the general governing equations for the fretting contact problem of the piezoelectric half-plane acted upon by a rigid conducting punch. Since the fretting contact is frictional and loading history dependent, the analysis is often divided into the normal loading process and tangential loading process. These two processes are discussed in the next two sections.

3. Normal loading

For the first step of fretting contact analysis, we consider the normal contact with a monotonically increasing normal load P to form a contact region $-a \leq x \leq a$, while the tangential load Q is neglected

as shown in Figure 2. Due to two dissimilar contact bodies pressed together under the action of a purely normal load, the corresponding surface particles will undergo different tangential displacements, and this relative tangential motion will lead to the development of the tangential traction at the interface. That is to say, an applied normal load will lead to both normal and tangential displacements. Therefore, the normal contact of two dissimilar bodies is fully coupled to the normal contact pressure and tangential traction. It is assumed that the whole contact region contains a centrally located stick region ($|x| \leq b$) between two slip regions ($b < |x| \leq a$) in which Coulomb's friction law is applied. The slip direction must also be consistent with the direction of the frictional force in the slip regions, which means that the slips in both slip regions are in opposite directions.

Referring to [Nowell et al. 1988] and [Hills et al. 1993], the tangential traction in the slip and stick regions is written as

$$q(x) = \begin{cases} -\eta p(x) \text{sign}(x) & b < |x| \leq a, \\ -\eta p(b)(x/b) + q^*(x) & |x| \leq b, \end{cases} \quad (17)$$

where $q^*(x)$ is an unknown function equal to zero at $x = \pm b$.

For a cylindrical punch, the derivative of u_{z0} may be approximately represented as [Johnson 1985]

$$\frac{\partial u_{z0}}{\partial x} = \frac{x}{R}, \quad |x| \leq a. \quad (18)$$

The surface electric potential ϕ_0 is a constant inside the contact region, so we have

$$\frac{\partial \phi_0}{\partial x} = 0, \quad |x| \leq a. \quad (19)$$

Spence [1973] proposed the self-similarity assumption that the stress fields were self-similar at each stage during monotonically increasing normal loading. In the inner stick region, the prior prestrain of surface points before they enter the stick region is proportional to $|x|$ as given by

$$\frac{\partial u_{x0}}{\partial x} = C|x|, \quad |x| \leq b, \quad (20)$$

where C is unknown and denotes the slope of the tangential displacement gradient at this stage. In the slip regions $b < |x| \leq a$, $\partial u_{x0}/\partial x$ cannot be specified.

With the aid of (18) and (19), (12) and (13) can be rewritten as

$$\frac{1}{\pi} \int_{-a}^a \frac{p(t)}{t-x} dt = \frac{f_{33}x}{\gamma_1 R} - i \frac{\gamma_2}{\gamma_1} q(x), \quad |x| \leq a, \quad (21)$$

$$-\frac{f_{23}}{\pi} \int_{-a}^a \frac{g(t)}{t-x} dt = \frac{x}{R} + \frac{f_{21}}{\pi} \int_{-a}^a \frac{p(t)}{t-x} dt + i f_{22} q(x), \quad |x| \leq a, \quad (22)$$

where

$$\gamma_1 = f_{31}f_{23} - f_{21}f_{33}, \quad \gamma_2 = f_{32}f_{23} - f_{22}f_{33}.$$

For the conducting cylindrical punch, the contact pressure is smooth at $x = \pm a$, while the electric charge can be divided into two parts [Ke et al. 2008]

$$g(x) = g_1(x) + g_2(x), \quad (23)$$

where $g_1(x)$ is induced by the normal load P and is smooth at $x = \pm a$, while $g_2(x)$ is induced by the constant electric potential ϕ_0 and has the square root singularity at both ends.

Then, by representing $t = a\theta$ and $x = a\tau$ ($-1 \leq (\tau, \theta) \leq 1$), (21), (14), (22) and (16) are normalized as

$$\frac{1}{\pi} \int_{-1}^1 \frac{p(\theta)}{\theta - \tau} d\theta = h_0(\tau), \tag{24}$$

$$\int_{-1}^1 p(\theta) d\theta = \frac{P}{a}, \tag{25}$$

$$-\frac{f_{23}}{\pi} \int_{-1}^1 \frac{g_1(\theta)}{\theta - \tau} d\theta = h_1(\tau), \tag{26}$$

$$\int_{-1}^1 g_1(\theta) d\theta = \frac{\Gamma_1}{a}, \tag{27}$$

$$-\frac{f_{23}}{\pi} \int_{-1}^1 \frac{g_2(\theta)}{\theta - \tau} d\theta = 0, \tag{28}$$

$$\int_{-1}^1 g_2(\theta) d\theta = \frac{\Gamma - \Gamma_1}{a}, \tag{29}$$

where

$$h_0(\tau) = \frac{f_{33}a\tau}{\gamma_1 R} - i \frac{\gamma_2}{\gamma_1} q(\tau), \tag{30}$$

$$h_1(\tau) = \frac{a\tau}{R} + \frac{f_{21}}{\pi} \int_{-1}^1 \frac{p(\theta)}{\theta - \tau} d\theta + i f_{22} q(\tau). \tag{31}$$

Next, substituting (17) into (11) yields the equation about $q^*(x)$,

$$\frac{1}{\pi} \int_{-b}^b \frac{q^*(t)}{t - x} dt = N_1(x), \quad |x| \leq b, \tag{32}$$

where

$$N_1(x) = -\frac{C|x|}{f_{12}} - i \frac{f_{11}}{f_{12}} p(x) - i \frac{f_{13}}{f_{12}} g(x) + \frac{\eta}{\pi} \int_b^a \frac{p(t)}{t - x} dt - \frac{\eta}{\pi} \int_{-a}^{-b} \frac{p(t)}{t - x} dt + \frac{\eta p(b)}{b\pi} \int_{-b}^b \frac{t}{t - x} dt. \tag{33}$$

By introducing the normalized quantities $t = b\kappa$ and $x = b\alpha$, (32) may be expressed as

$$\frac{1}{\pi} \int_{-1}^1 \frac{q^*(\kappa)}{\kappa - \alpha} d\kappa = N_1(\alpha), \quad |\alpha| \leq 1. \tag{34}$$

In addition, the following consistency condition should be satisfied [Muskhelishvili 1958]:

$$\int_{-1}^1 \frac{N_1(\zeta)}{\sqrt{1 - \zeta^2}} d\zeta = 0. \tag{35}$$

Using the method of Erdogan and Gupta [1972], this integral equation may be reduced to a set of linear equations that satisfy the consistency condition (35). Through setting $q^*(\kappa) = \varphi(\kappa)\sqrt{1 - \kappa^2}$, we

can discretize (34) to give

$$\sum_{l=1}^M \frac{(1 - \kappa_l^2)\varphi(\kappa_l)}{(M+1)(\kappa_l - \alpha_r)} = N_1(\alpha_r), \quad |\alpha_r| \leq 1, \quad (36)$$

where $\kappa_l = \cos[l\pi/(M+1)]$, $\alpha_r = \cos[(2r-1)\pi/2(M+1)]$, $r = 1, 2, \dots, M+1$, and M is the total number of the discrete points of $\varphi(\kappa_l)$ in $(-1, 1)$. By setting $p(\theta) = \psi(\theta)\sqrt{1-\theta^2}$ and $g_1(\theta) = \lambda(\theta)\sqrt{1-\theta^2}$, (24)–(27) are also discretized as

$$\sum_{l=1}^M \frac{(1 - \theta_l^2)\psi(\theta_l)}{(M+1)(\theta_l - \tau_r)} = h_0(\tau_r), \quad |\tau_r| \leq 1, \quad (37)$$

$$\sum_{l=1}^M \frac{(1 - \theta_l^2)\psi(\theta_l)}{M+1} = \frac{P}{a\pi}, \quad (38)$$

$$\sum_{l=1}^M -\frac{f_{23}(1 - \theta_l^2)\lambda(\theta_l)}{(M+1)(\theta_l - \tau_r)} = h_1(\tau_r), \quad |\tau_r| \leq 1, \quad (39)$$

$$\sum_{l=1}^M \frac{(1 - \theta_l^2)\lambda(\theta_l)}{M+1} = \frac{\Gamma_1}{a\pi}, \quad (40)$$

where $\theta_l = \cos[l\pi/(M+1)]$, $\tau_r = \cos[(2r-1)\pi/2(M+1)]$, $r = 1, 2, \dots, M+1$, where M is the total number of the discrete points of $\psi(\theta_l)$ and $\lambda(\theta_l)$ in $(-1, 1)$.

Because $g_2(x)$ has the square root singularity at both ends, we can set $g_2(\theta) = \vartheta(\theta)/\sqrt{1-\theta^2}$. Then (28) and (29) can be reduced to

$$\frac{1}{M} \sum_{l=1}^M \frac{f_{23}\vartheta(\theta_l)}{(\theta_l - \tau_r)} = 0, \quad |\tau_r| \leq 1, \quad (41)$$

$$\frac{1}{M} \sum_{l=1}^M \vartheta(\theta_l) = \frac{\Gamma - \Gamma_1}{a\pi}, \quad (42)$$

where $\theta_l = \cos[(2l-1)\pi/2M]$, $\tau_r = \cos[r\pi/M]$, $r = 1, 2, \dots, M-1$, where M is the total number of the discrete points of $\vartheta(\theta_l)$ in $(-1, 1)$.

In (36), (37), (39) and (41), we have $4M+2$ equations and $4M+3$ unknowns, $\varphi(\kappa_1), \dots, \varphi(\kappa_M)$, $\psi(\theta_1), \dots, \psi(\theta_M)$, $\lambda(\theta_1), \dots, \lambda(\theta_M)$, $\vartheta(\theta_1), \dots, \vartheta(\theta_M)$, a , b and C ; the problem is also underconstrained. As we know, the tangential traction must be continuous at the stick-slip interface, which leads to the requirements $\varphi(\pm 1) = 0$ [Keer and Farris 1987; Hanson et al. 1989]. This condition can therefore be utilized to determine b and $q(x)$, to make the analysis self-contained. This technique would require a sequence of iteration, which can be specified as follows:

- (1) Input the values of a and b . The frictionless solutions of the contact pressure $p^0(\theta)$ and electric charge $g^0(\theta)$ from Ke et al. [2008] are selected as the initial values for $p(\theta)$ and $g(\theta)$.
- (2) Solve (36) to obtain the tangential traction $q^1(\kappa)$ for $q(\kappa)$, and substitute $q^1(\kappa)$ into (37), (39) and (41). Then, $p^1(\theta)$ and $g^1(\theta)$ can be solved from this set of equations.

- (3) Calculate $\varphi(\pm 1)$ from (36). If $\varphi(\pm 1) = 0$, go to the next step; if $\varphi(\pm 1) \neq 0$, return to steps 1 and 2. Then, the new values must be selected for b and a , and the procedure is repeated.
- (4) Calculate $p^n(\theta)$, $g^n(\theta)$ and $q^n(\kappa)$ (the superscript n denotes the n -th iteration), together with C , which satisfy (36), (37), (39) and (41) and are the solutions of the coupled normal contact problem. Then, we can get P and Γ from (38), (40) and (42).

4. Tangential loading

4.1. A monotonically increasing tangential load. At the end of the normal loading phase, the whole contact region is divided into the inner stick region $|x| \leq b$ and two outer slip regions $b < x \leq a$ and $-a \leq x < -b$. Then, we apply a cyclic tangential load Q ($|Q| < \eta P$) to the punch as shown in Figure 1. The tangential loading history is depicted in Figure 3 to define the tangential load Q as a function of time. In the first step of the tangential loading problem, the cylindrical punch is acted upon by a constant normal load P , and then subjected to a monotonically increasing tangential load from zero to a maximum value Q_{\max} , i.e., point A in Figure 3.

The normal contact pressure, tangential traction and electric charge distributions at the end of the normal loading phase can be found from the fully coupled normal contact in previous section. The resulting values of the relative tangential displacement gradient $\partial u_{x0}/\partial x$ in the whole contact region are then calculated using (11) and stored. We expect an inner stick region at the interval $-b_1 \leq x \leq b_2$ bordered by two slip regions ($-a \leq x < -b_1$ and $b_2 < x \leq a$) with the same slip direction as shown in Figure 1. In the slip regions, the tangential traction $q(x)$ is strictly related to the local normal contact pressure $p(x)$ by Coulomb’s friction law. Hence, (11) is rewritten as

$$\frac{1}{\pi} \int_{-b_1}^{b_2} \frac{q^{**}(t)}{t-x} dt = N_2(x), \quad -b_1 \leq x \leq b_2, \tag{43}$$

where

$$q^{**}(x) = -\eta p(x) + q(x), \tag{44}$$

$$N_2(x) = -\frac{1}{f_{12}} \frac{\partial u_{x0}}{\partial x} - \frac{if_{11}}{f_{12}} p(x) - \frac{if_{13}}{f_{12}} g(x) - \frac{\eta}{\pi} \int_{-a}^a \frac{p(t)}{t-x} dt. \tag{45}$$

Once the tangential load is applied, the normal contact pressure and electric charge distributions may become asymmetric. Therefore, the contact patch may be not central about the center-line of the punch

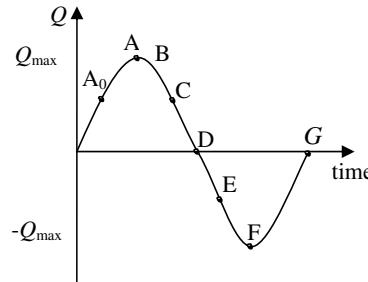


Figure 3. Load history of the tangential load Q as a function of time.

which allows for an eccentricity e between the center-line and the origin [Nowell et al. 1988]. Thus, (21) and (22) have the form

$$\frac{1}{\pi} \int_{-a}^a \frac{p(t)}{t-x} dt = \frac{f_{33}(x-e)}{\gamma_1 R} - i \frac{\gamma_2}{\gamma_1} q(x), \quad |x| \leq a, \quad (46)$$

$$-\frac{f_{23}}{\pi} \int_{-a}^a \frac{g(t)}{t-x} dt = \frac{x-e}{R} + \frac{f_{21}}{\pi} \int_{-a}^a \frac{p(t)}{t-x} dt + i f_{22} q(x), \quad |x| \leq a. \quad (47)$$

In addition, the static equilibrium for the normal contact pressure and tangential traction must be satisfied by (14) and (15). Substituting (44) and (14) into (15) yields

$$\int_{-b_1}^{b_2} q^{**}(t) dt = Q - \eta P. \quad (48)$$

Introducing the following normalized quantities

$$t = \frac{b_1 + b_2}{2} \kappa + \frac{b_2 - b_1}{2}, \quad x = \frac{b_1 + b_2}{2} \alpha + \frac{b_2 - b_1}{2}, \quad (49)$$

Equations (43) and (48) may be expressed in the form of

$$\frac{1}{\pi} \int_{-1}^1 \frac{q^{**}(\kappa)}{\kappa - \alpha} d\kappa = N_2(\alpha), \quad |\alpha| \leq 1, \quad (50)$$

$$\int_{-1}^1 q^{**}(\kappa) d\kappa = \frac{2(Q - \eta P)}{b_1 + b_2}. \quad (51)$$

Using (23), (46) and (47) are normalized by introducing $t = a\theta$ and $x = a\tau$,

$$\frac{1}{\pi} \int_{-1}^1 \frac{p(\theta)}{\theta - \tau} d\theta = h_2(\tau), \quad |\tau| \leq 1, \quad (52)$$

$$-\frac{f_{23}}{\pi} \int_{-1}^1 \frac{g_1(\theta)}{\theta - \tau} d\theta = h_3(\tau), \quad |\tau| \leq 1, \quad (53)$$

where

$$h_2(\tau) = \frac{f_{33}(a\tau - e)}{\gamma_1 R} - i \frac{\gamma_2}{\gamma_1} q(\tau), \quad (54)$$

$$h_3(\tau) = \frac{a\tau - e}{R} + \frac{f_{21}}{\pi} \int_{-1}^1 \frac{p(\theta)}{\theta - \tau} d\theta + i f_{22} q(\tau). \quad (55)$$

Equations (52) and (53) are also discretized by setting $p(\theta) = \psi(\theta)\sqrt{1-\theta^2}$ and $g_1(\theta) = \lambda(\theta)\sqrt{1-\theta^2}$ to give

$$\sum_{l=1}^M \frac{(1-\theta_l^2)\psi(\theta_l)}{(M+1)(\theta_l - \tau_r)} = h_2(\tau_r), \quad |\tau_r| \leq 1, \quad (56)$$

$$\sum_{l=1}^M -\frac{f_{23}(1-\theta_l^2)\lambda(\theta_l)}{(M+1)(\theta_l - \tau_r)} = h_3(\tau_r), \quad |\tau_r| \leq 1, \quad (57)$$

where $\theta_l = \cos[l\pi/(M+1)]$, $\tau_r = \cos[(2r-1)\pi/2(M+1)]$, $r = 1, 2, \dots, M+1$, where M is the total number of the discrete points of $\psi(\theta_l)$ and $\lambda(\theta_l)$ in $(-1, 1)$.

Equations (50) and (51) are also discretized by setting $q^{**}(\kappa) = \varphi(\kappa)\sqrt{1-\kappa^2}$ to give

$$\sum_{l=1}^M \frac{(1-\kappa_l^2)\varphi(\kappa_l)}{(M+1)(\kappa_l-\alpha_r)} = N_2(\alpha_r), \quad |\alpha_r| \leq 1, \quad (58)$$

$$\sum_{l=1}^M \frac{(1-\kappa_l^2)\varphi(\kappa_l)}{M+1} = \frac{2(Q-\eta P)}{(b_1+b_2)\pi}, \quad (59)$$

where $\kappa_l = \cos[l\pi/(M+1)]$, $\alpha_r = \cos[(2r-1)\pi/2(M+1)]$, $r = 1, 2, \dots, M+1$, and M is the total number of the discrete points of $\varphi(\kappa_l)$ in $(-1, 1)$. In (41), (56), (57) and (58), there are $4M+2$ equations for $4M+3$ unknowns, $\varphi(\kappa_1), \dots, \varphi(\kappa_M)$, $\psi(\theta_1), \dots, \psi(\theta_M)$, $\lambda(\theta_1), \dots, \lambda(\theta_M)$, $\vartheta(\theta_1), \dots, \vartheta(\theta_M)$, b_1 , b_2 and e . It should be noted that the discretization of (58) yields $M+1$ equations for M unknowns $\varphi(\kappa_l)$, since in this case there is no constant C to be determined, as the stick zone is receding. The iterative procedure is given below:

- (1) Input a value of b_1 and a trial value of b_2 , and drop the $(M+1)$ -th equation of (58).
- (2) Compute the solution of the coupled equations (41), (56), (57) and (58) by using the iterative procedure described in Section 3.
- (3) Check whether the solution satisfies the $(M+1)$ -th equation of (58). If it satisfies, we obtain the consistent solution; then go to the next step. Otherwise, a new value of b_2 must be chosen for step 1 and the iteration procedure is continued till the consistent solution is achieved.
- (4) Compute the applied normal load P , electric charge Γ and tangential load Q from (38), (40), (42) and (59).

4.2. A cyclic tangential load. In the previous subsection, we analyzed the tangential load Q , which increased monotonically from 0 to Q_{\max} . However, the tangential load is generally cyclic between limits in fretting fatigue. So, we further consider a cyclic tangential load varying between the limits $\pm Q_{\max}$ applied to the rigid conducting cylindrical punch. Starting immediately at unloading, the pressure cannot sustain the stick at the outer edge of contact where the tangential traction becomes $q(x) = -\eta p(x)$. Since the frictional contact problem depends on the loading history, the contact tractions and electric charge can be first obtained at the end of the monotonically increasing tangential loading phase ($Q = Q_{\max}$); $\partial u_{x0}/\partial x$ can be calculated and stored by considering (43). Equation (11) is resolved in the new stick region, $-c_1 \leq x \leq c_2$, and reverse slip regions, $-a \leq x < -c_1$ and $c_2 < x \leq a$, and thus can be expressed as

$$\frac{1}{\pi} \int_{-c_1}^{c_2} \frac{q^{***}(t)}{t-x} dt = N_3(x), \quad -c_1 \leq x \leq c_2, \quad (60)$$

where

$$q^{***}(x) = q(x) + \eta p(x), \quad (61)$$

$$N_3(x) = -\frac{1}{f_{12}} \frac{\partial u_{x0}}{\partial x} - i \frac{f_{11}}{f_{12}} p(x) - i \frac{f_{13}}{f_{12}} g(x) + \frac{\eta}{\pi} \int_{-a}^a \frac{p(t)}{t-x} dt. \quad (62)$$

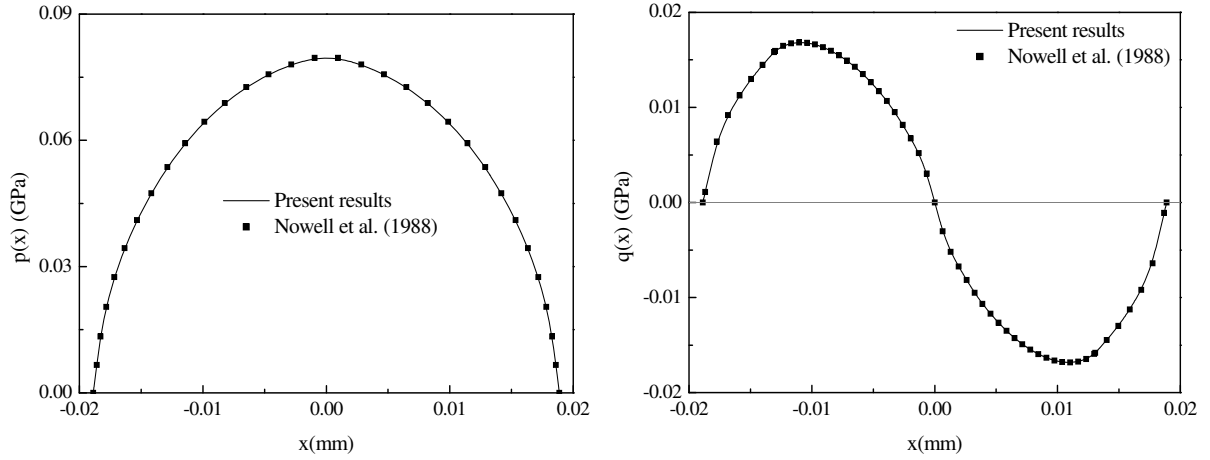


Figure 4. Comparison of the present results with the results obtained in [Nowell et al. 1988]: (left) normal contact pressure; and (right) tangential traction.

In addition, the static equilibrium for the contact tractions must satisfy

$$\int_{-c_1}^{c_2} q^{***}(t) dt = Q + \eta P. \quad (63)$$

Equation (60) is also solved together with (41), (56) and (57) by using the iterative procedure developed in Section 4.1. Note that this process may be continued for the reverse loading phase (DF in Figure 3), reverse unloading phase (FG in Figure 3) and other loading cycles.

5. In-plane stress and in-plane electric displacement

After we obtain the tangential contact stress $\sigma_{zx0} = -q(x)$, along with the normal contact stress $\sigma_{zz0} = -p(x)$ and electrical displacement $D_{z0} = -g(x)$ for the normal and tangential loading processes, the in-plane stress σ_{xx0} and in-plane electric displacement D_{x0} at the contact surface can be solved as

$$\sigma_{xx0}(x) = -(\Delta_1 + if_{11}\Delta_3)p(x) - (\Delta_2 + if_{13}\Delta_3)g(x) - \frac{\Delta_3 f_{12}}{\pi} \int_{-a}^a \frac{q(t)}{t-x} dt, \quad (64)$$

$$D_{x0}(x) = -\left(\frac{e_{15}}{c_{44}} - if_{32}\Delta_4\right)q(x) + \frac{\Delta_4 f_{31}}{\pi} \int_{-a}^a \frac{p(t)}{t-x} dt + \frac{\Delta_4 f_{33}}{\pi} \int_{-a}^a \frac{g(t)}{t-x} dt, \quad (65)$$

where

$$\Delta_1 = \frac{e_{31}e_{33} + c_{13}\epsilon_{33}}{e_{33}^2 + c_{33}\epsilon_{33}}, \quad \Delta_2 = \frac{c_{13}e_{33} - c_{33}e_{31}}{e_{33}^2 + c_{33}\epsilon_{33}},$$

$$\Delta_3 = \frac{c_{11}e_{33}^2 - c_{13}^2\epsilon_{33} + c_{33}e_{31}^2 + c_{11}c_{33}\epsilon_{33} - 2c_{13}e_{31}e_{33}}{e_{33}^2 + c_{33}\epsilon_{33}}, \quad \Delta_4 = \frac{e_{15}^2}{c_{44}} + \epsilon_{11}.$$

6. Results and discussion

Before the analysis of the fretting contact of piezoelectric materials, we first verify the effectiveness of the present method. If we neglect the anisotropy and piezoelectric effect of materials, the present contact

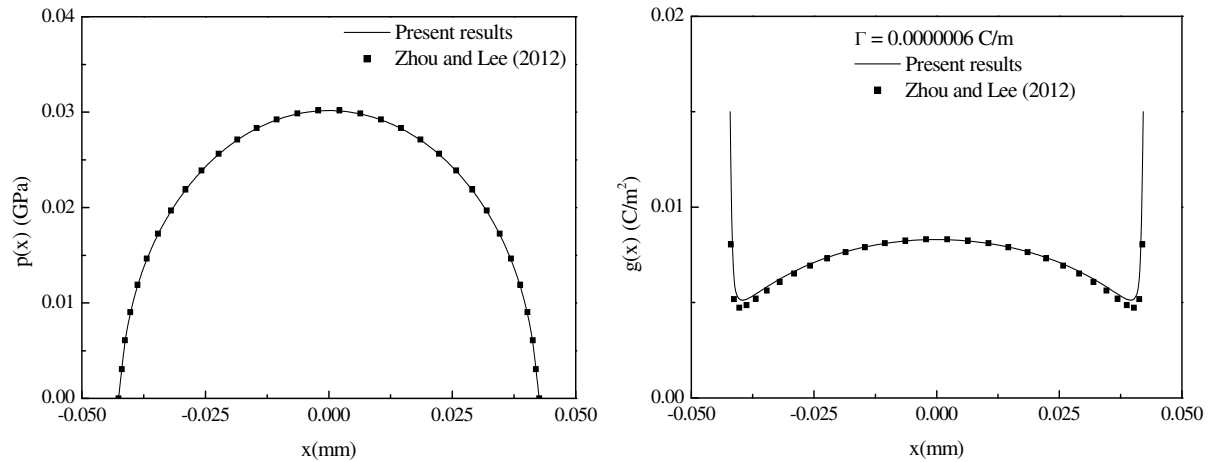


Figure 5. Comparison of the present results with the results obtained in [Zhou and Lee 2012]: (left) normal contact pressure; and (right) electric charge distributions.

problem can be easily reduced to the fretting contact of an isotropic elastic half-plane under a rigid cylindrical punch. Figure 4 plots the normal contact pressure and tangential traction for the coupled normal contact with $\eta = 0.3$, $R = 10$ mm and $P = 2.24 \cdot 10^3$ N/m. The elastic half-plane is made of aluminum with the shear modulus $\mu = 27.3$ GPa and Poisson's ratio $\nu = 0.3$. The results in [Nowell et al. 1988] are also provided in Figure 4 for a direct comparison. It is observed that the present results agree well with the results given in [Nowell et al. 1988].

If we neglect the friction, the present contact problem is reduced to the frictionless contact of piezoelectric materials. Zhou and Lee [2012] obtained the exact solutions for the frictionless contact of a piezoelectric half-plane under a rigid conducting cylindrical punch. Figure 5 presents the normal contact pressure and electric charge distributions for the frictionless contact of piezoelectric materials with $R = 60$ mm, $P = 2000$ N/m and $\Gamma = 6 \cdot 10^{-7}$ C/m. The present results show good agreement with the exact solutions.

In what follows, we will discuss the fretting contact behavior of a piezoelectric half-plane under a rigid conducting cylindrical punch. The half-plane is made of piezoceramic PZT-4 whose electromechanical properties are listed in Table 1 [Ke et al. 2008]. Unless otherwise stated, the resultant normal load, resultant electric charge and radius of the punch are selected as $P = 2000$ N/m, $\Gamma = 6 \cdot 10^{-7}$ C/m and $R = 60$ mm. Note that Su et al. [2015] studied the fretting contact of a piezoelectric half-plane under an insulating punch. Their results are also given in Figures 8, 9, 10, 16 and 19 to show the effect of the conductivity of the punch.

6.1. Normal loading. Figure 6 plots the effect of the friction coefficient η on the normal contact pressure $p(x)$, electric charge $g(x)$ and tangential traction $q(x)$. As can be expected, the electric charge is singular at the edge of the contact region, whereas the normal contact pressure and tangential traction are quite smooth. It is observed that $p(x)$ and $g(x)$ are symmetric, and $q(x)$ is antisymmetric with respect to $x = 0$. The friction coefficient has a slight effect on $p(x)$ and $g(x)$. However, it has a marked effect on $q(x)$. The peak value of $q(x)$ occurs at the interface between the stick region and slip region, and increases rapidly with the increase of η .

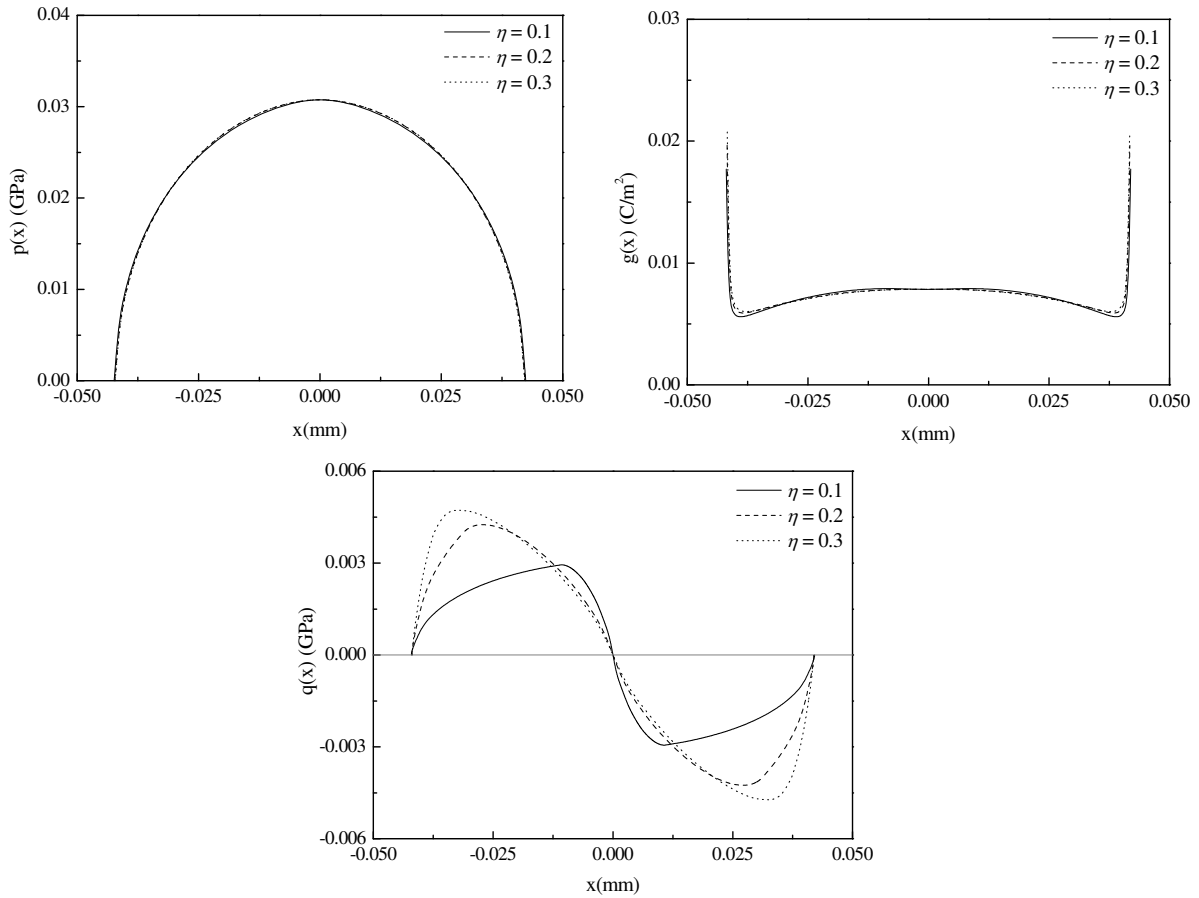


Figure 6. The effect of the friction coefficient η on the (left) normal contact pressure, (right) electric charge distributions and (bottom) tangential traction with $R = 60$ mm, $P = 2000$ N/m and $\Gamma = 6 \cdot 10^{-7}$ C/m.

c_{11} (GPa)	c_{13} (GPa)	c_{33} (GPa)	c_{44} (GPa)
139	74.3	115	25.6
e_{31} (C/m ²)	e_{33} (C/m ²)	e_{15} (C/m ²)	
-5.2	15.1	12.7	
ϵ_{11} (10^{-10} C/Vm)	ϵ_{33} (10^{-10} C/Vm)		
64.61	56.2		

Table 1. Piezoelectric material properties of PZT-4.

The effect of the friction coefficient η on the in-plane stress σ_{xx0} and in-plane electric displacement D_{x0} is given in Figure 7. The in-plane stress σ_{xx0} is symmetric with $x = 0$ and compressive at all regions. The maximum value of σ_{xx0} increases with the decrease of η , and occurs at the interface between the stick region and slip region. The in-plane electric displacement D_{x0} is insensitive to the friction coefficient. It

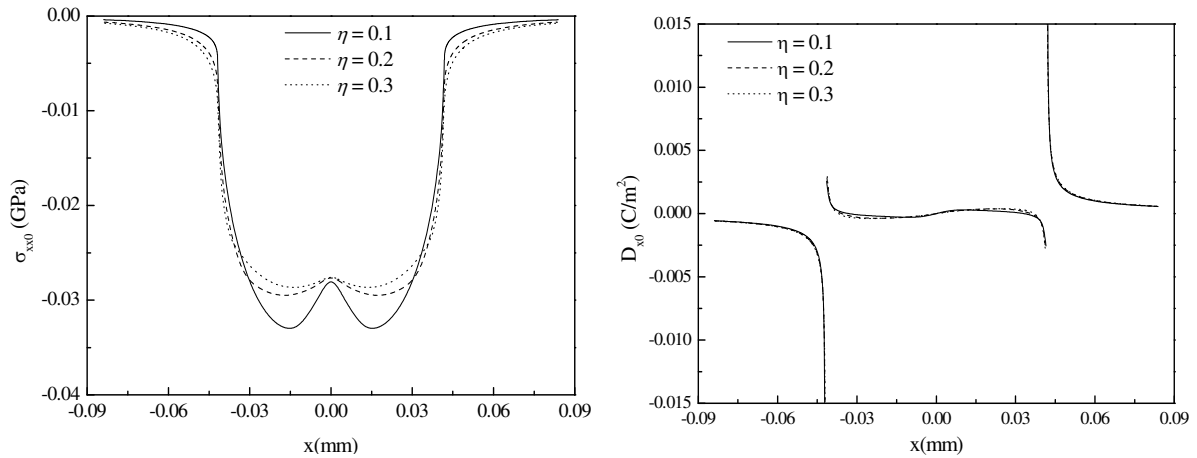


Figure 7. The effect of the friction coefficient η on the (left) in-plane stress σ_{xx0} and (right) in-plane electric displacement D_{x0} with $R = 60$ mm, $P = 2000$ N/m and $\Gamma = 6 \cdot 10^{-7}$ C/m.

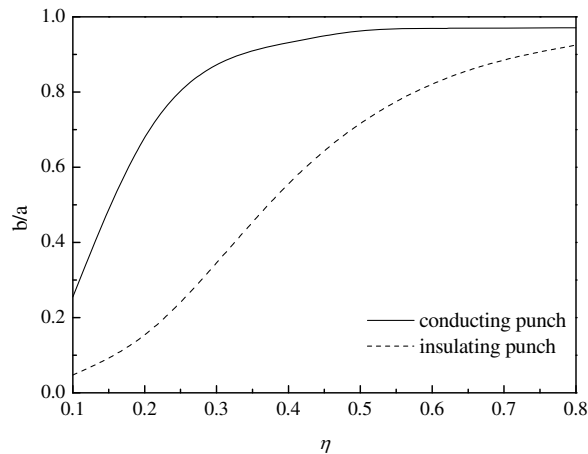


Figure 8. The relations between the stick region size and the friction coefficient with $R = 60$ mm, $P = 2000$ N/m and $\Gamma = 6 \cdot 10^{-7}$ C/m.

has the antisymmetric distribution with the positive value at the region $x > a$ and negative value at the region $x < a$. The maximum value of D_{x0} occurs at the two edges of the contact region.

Figure 8 depicts the relation between the stick region size b/a and friction coefficient η for both insulating and conducting punches. For both punches, the value of b/a increases with the increase of η , and is close to the value of fully adhesive contact (i.e., $b/a \approx 1$) for large η . It can be concluded that the higher the friction coefficient is the less likely the slip occurs. It is found that the conducting punch has a greater value of b/a than the insulating punch for a given η . Therefore, the conductivity of the punch has a significant effect on the fretting contact behavior of piezoelectric materials.

Figure 9 presents the relation between the slope of the tangential displacement gradient C and the friction coefficient η for both insulating and conducting punches. With the increase of η , the value of

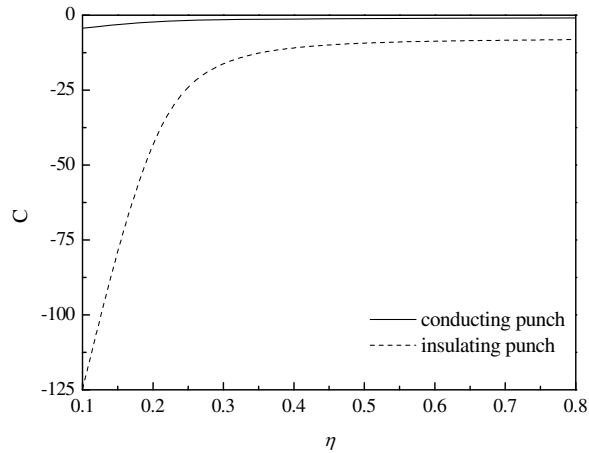


Figure 9. The relations between the slope of the tangential displacement gradient and the friction coefficient with $R = 60$ mm, $P = 2000$ N/m and $\Gamma = 6 \cdot 10^{-7}$ C/m.

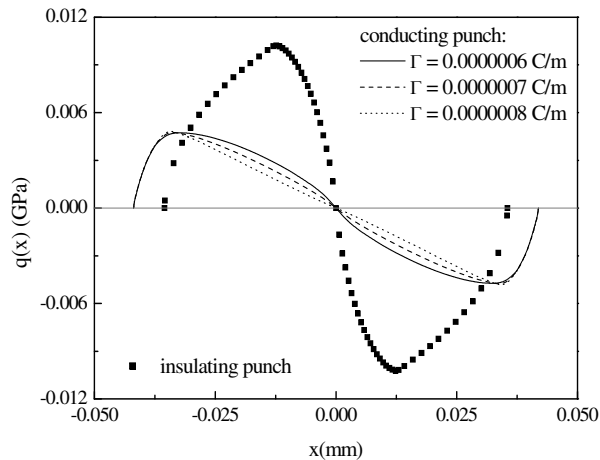


Figure 10. The effect of the resultant electric charge Γ on the tangential traction with $R = 60$ mm, $\eta = 0.3$, $P = 2000$ N/m.

C decreases rapidly when $\eta < 0.3$ (especially for the insulating punch), and then changes slightly when $0.3 \leq \eta \leq 0.8$. Moreover, the value C of the insulating punch is larger than that of the conducting punch for a given η .

Figure 10 analyzes the effect of the resultant electric charge Γ on the tangential traction for both insulating and conducting punches with $\eta = 0.3$. We found that the peak value of $q(x)$ for the insulating punch is greater than that of the conducting punch, but the size of the stick region is smaller than that of the conducting punch. With the increase of Γ , the value of $q(x)$ decreases at the stick region and changes slightly at the slip region. The results indicate that the insulation of the punch may lead to a concentration of the tangential traction, which may cause a serious influence on the fretting contact damage.

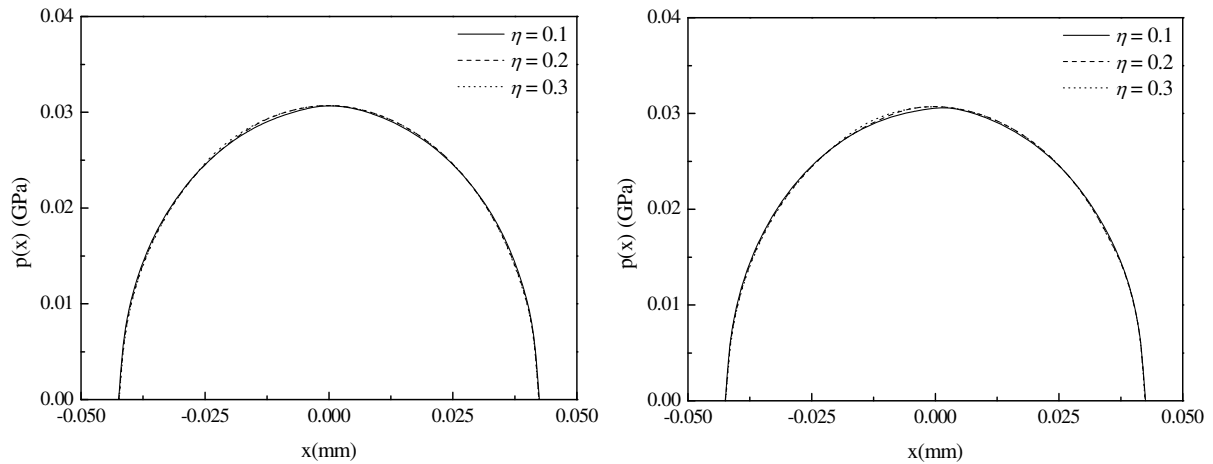


Figure 11. Normal contact pressure during monotonically increasing tangential loading with $R = 60$ mm, $P = 2000$ N/m and $\Gamma = 6 \cdot 10^{-7}$ C/m: (left) $Q/\eta P = 0.3$, point A_0 in Figure 3; and (right) $Q/\eta P = 0.5$, point A in Figure 3.

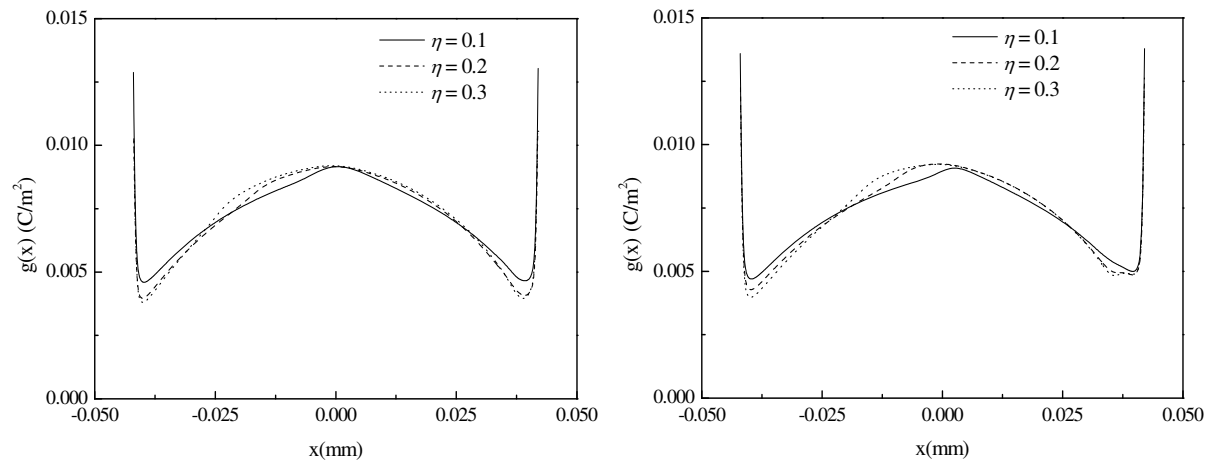


Figure 12. Electric charge distribution during monotonically increasing tangential loading with $R = 60$ mm, $P = 2000$ N/m and $\Gamma = 6 \cdot 10^{-7}$ C/m: (left) $Q/\eta P = 0.3$, point A_0 in Figure 3; and (right) $Q/\eta P = 0.5$, point A in Figure 3.

6.2. Tangential loading. Figures 11–13 discuss the effect of the friction coefficient η on the normal contact pressure $p(x)$, electric charge $g(x)$ and tangential traction $q(x)$ at the loading phase (points A_0 and A in Figure 3), respectively. Because of the action of the tangential load, the normal contact pressure, electric charge distributions and tangential traction are asymmetric during the loading phase. The friction coefficient has a minor effect on the normal contact pressure and electric charge distributions, but it has a significant effect on the tangential traction. It shows that the maximum value of the tangential traction increases with the increase of the friction coefficient and appears at the interface of the stick/slip region. Additionally, because the eccentricity e is very small, the normal contact pressure and electric charge

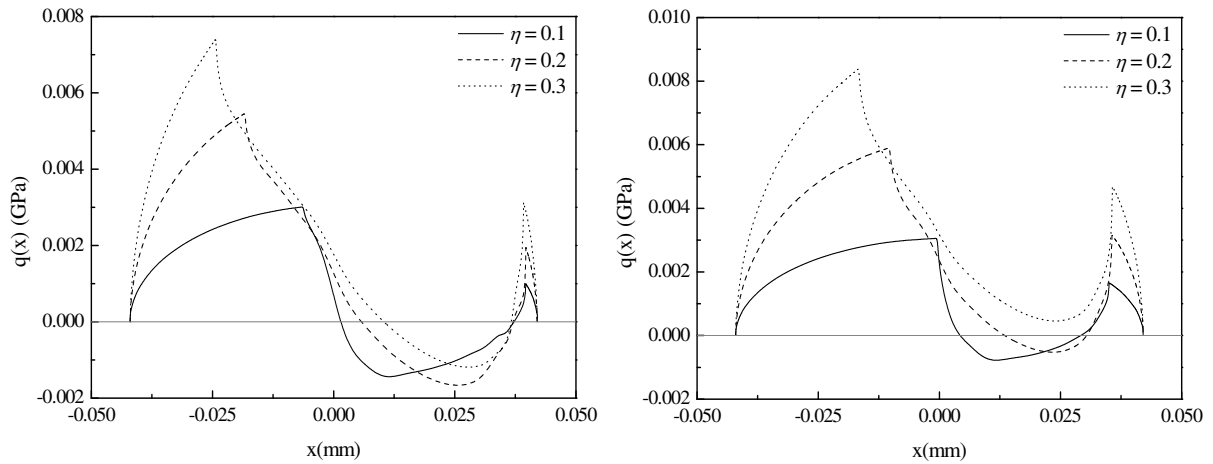


Figure 13. Tangential traction during monotonically increasing tangential loading with $R = 60$ mm, $P = 2000$ N/m and $\Gamma = 6 \cdot 10^{-7}$ C/m: (left) $Q/\eta P = 0.3$, point A_0 in Figure 3; and (right) $Q/\eta P = 0.5$, point A in Figure 3.

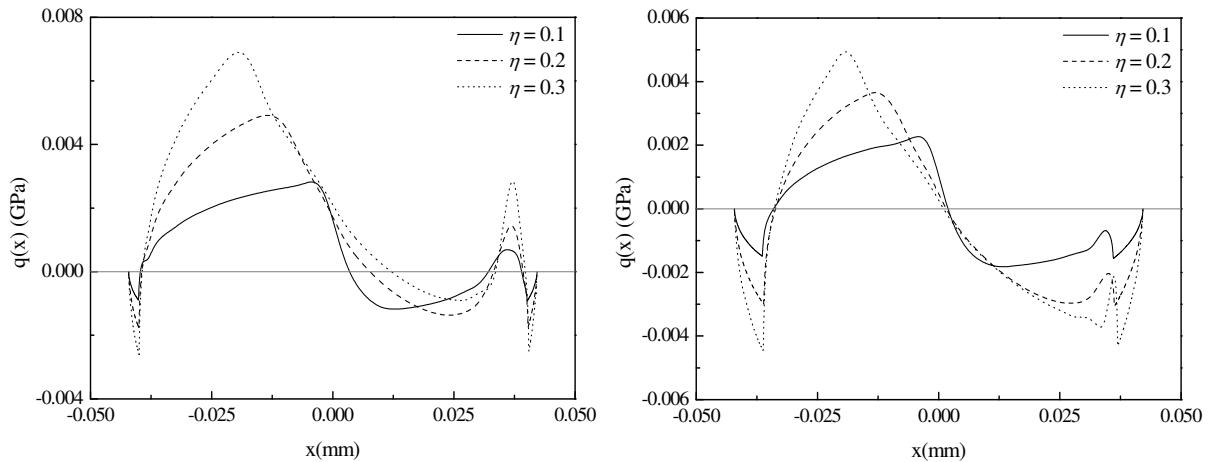


Figure 14. Tangential traction during cyclic tangential loading with $R = 60$ mm, $P = 2000$ N/m and $\Gamma = 6 \cdot 10^{-7}$ C/m: (left) $Q/\eta P = 0.3$, point C in Figure 3; and (right) $Q/\eta P = 0.0$, point D in Figure 3.

at the tangential loading phase is very close to those at the normal loading phase. Hence, the normal contact pressure and electric charge distributions will not be discussed in the following analysis.

Figures 14 and 15 analyze the effect of the friction coefficient η on the tangential traction at the unloading and reverse loading phases (points C, D, E and F in Figure 3). At first, near the two edges of the contact region, we see that the reverse slip occurs during the unloading phase; and the tangential traction becomes $q(x) = -\eta p(x)$. Due to the effect of the loading history, the distribution of the tangential traction becomes quite complex at the stick region, and a localized increase or decrease occurs at the interface of the stick/slip region during the unloading phase. Comparing Figure 13 (right) to Figure 15 (right), we

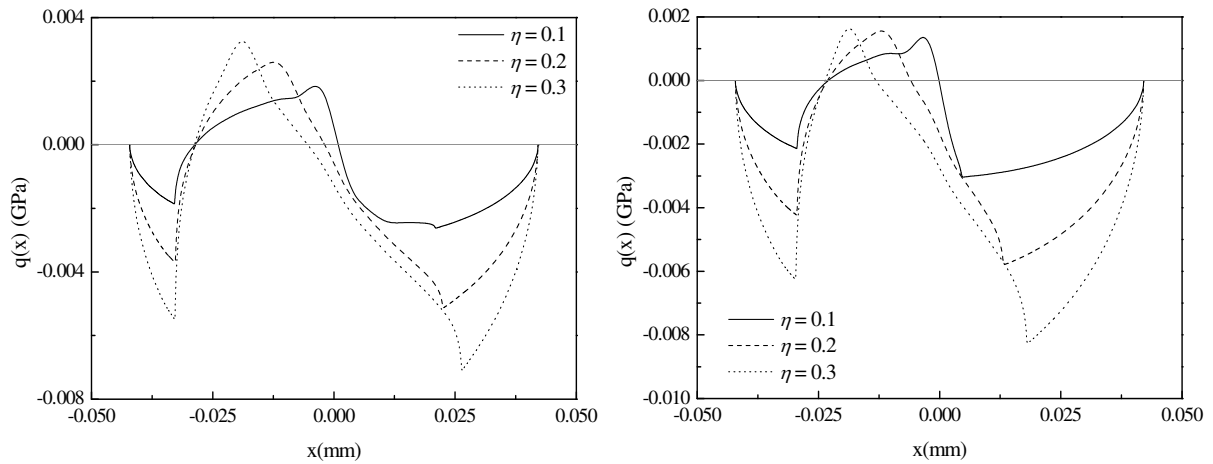


Figure 15. Tangential traction during cyclic tangential loading with $R = 60$ mm, $P = 2000$ N/m and $\Gamma = 6 \cdot 10^{-7}$ C/m: (left) $Q/\eta P = -0.3$, point E in Figure 3; and (right) $Q/\eta P = -0.5$, point F in Figure 3.

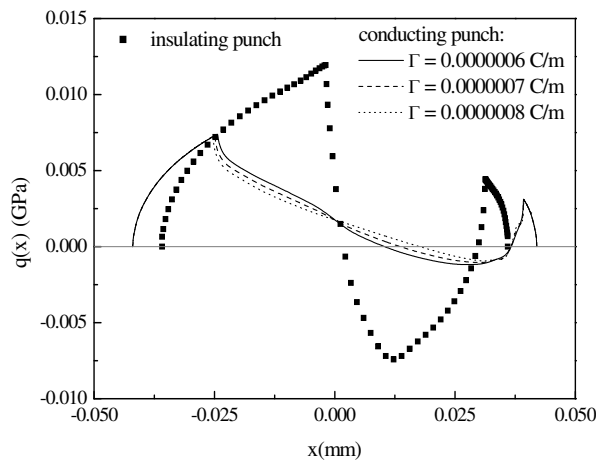


Figure 16. Tangential traction during monotonically increasing tangential loading with $R = 60$ mm, $P = 2000$ N/m, $\eta = 0.3$ and $Q/\eta P = 0.3$, point A_0 in Figure 3.

can observe that the distribution of tangential traction is completely reversed when the tangential load is completely reversed from $Q = Q_{max}$ to $Q = -Q_{max}$.

Figure 16 shows the effect of the resultant electric charge Γ on the tangential traction $q(x)$ during the loading phase (points A_0 in Figure 3) for both insulating and conducting punches. Similar to the normal loading phase, the peak value of $q(x)$ for the insulating punch is greater than that of the conducting punch during the tangential loading phase. With the increase in Γ , the value of $q(x)$ has a slight change at the stick region, and is almost unchanged at the slip region.

Figure 17 plots the effect of the friction coefficient η on the in-plane stress σ_{xx0} when $Q/\eta P = \pm 0.5$. For $Q/\eta P = 0.5$, σ_{xx0} is compressive at the region $x < 0$, but changes from compressive to tensile and

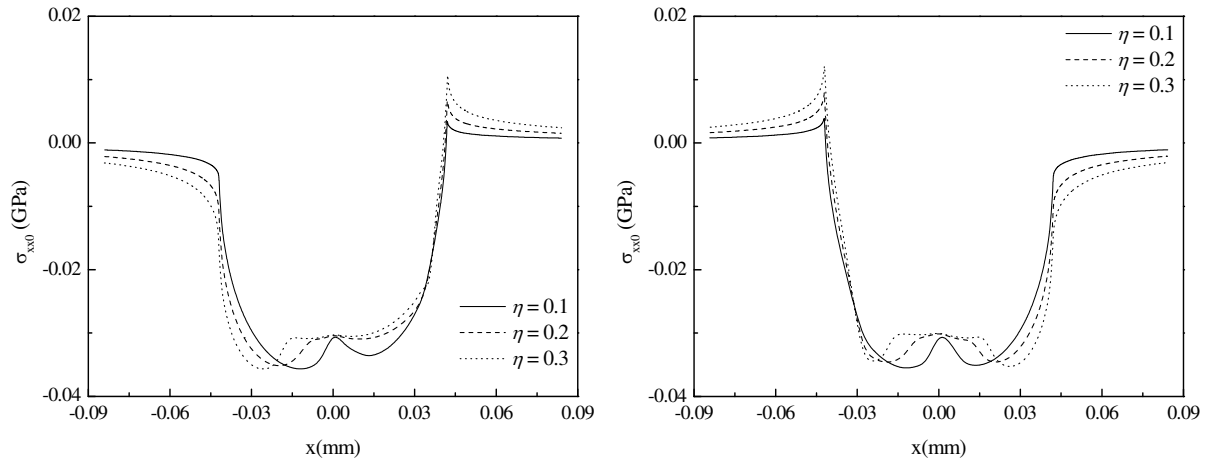


Figure 17. The effect of the friction coefficient η on the in-plane stress σ_{xx0} with $R = 60$ mm, $P = 2000$ N/m and $\Gamma = 6 \cdot 10^{-7}$ C/m: (left) $Q/\eta P = 0.5$, point A in Figure 3; and (right) $Q/\eta P = -0.5$, point F in Figure 3.

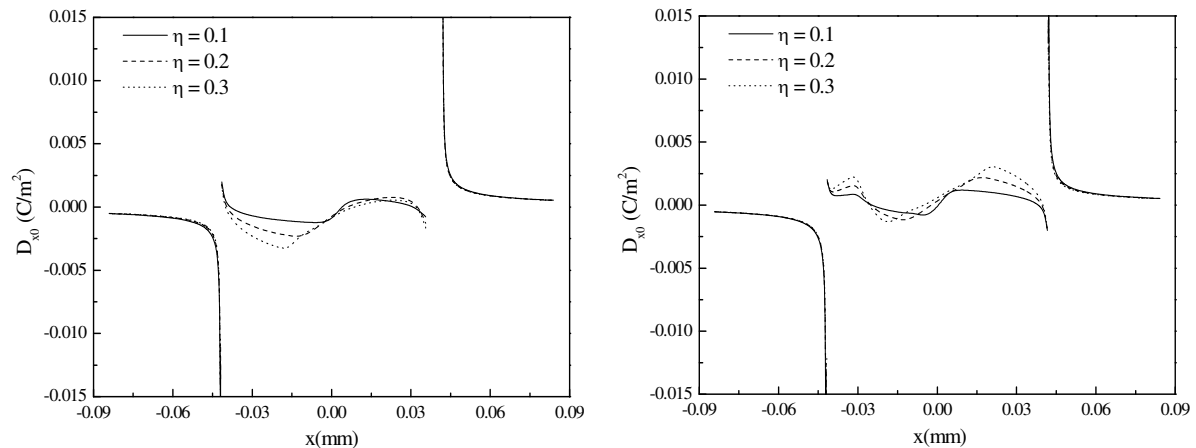


Figure 18. The effect of the friction coefficient η on the in-plane electric displacement D_{x0} with $R = 60$ mm, $P = 2000$ N/m and $\Gamma = 6 \cdot 10^{-7}$ C/m: (left) $Q/\eta P = 0.5$, point A in Figure 3; and (right) $Q/\eta P = -0.5$, point F in Figure 3.

increases as η increases throughout most of the region $x > 0$. The behavior of σ_{xx0} for $Q/\eta P = -0.5$ is opposite of that for $Q/\eta P = 0.5$. In particular, the maximum tensile stress σ_{xx0} increases with the increase of η , and occurs at $x = a$ for $Q/\eta P = 0.5$ and at $x = -a$ for $Q/\eta P = -0.5$. The maximum tensile stress implies the possible site of the fretting crack initiation.

Figure 18 analyzes the effect of the friction coefficient η on the in-plane electric displacement D_{x0} when $Q/\eta P = \pm 0.5$. During tangential loading phase, the in-plane electric displacement distribution is quite similar to that of the normal loading phase. The friction coefficient η also has little effect on the in-plane electric displacement.

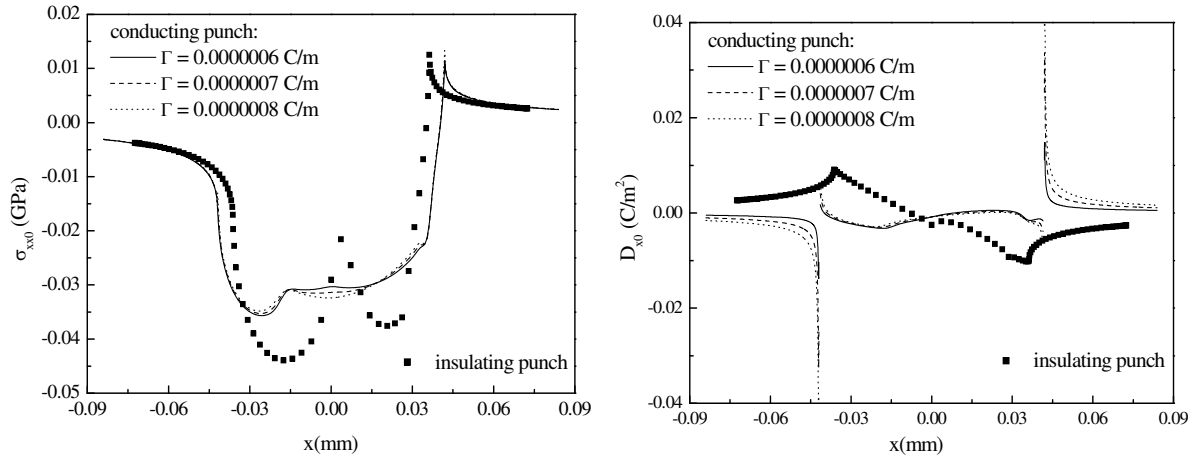


Figure 19. The effect of the resultant electric charge Γ on the (left) in-plane stress σ_{xx0} and (right) in-plane electric displacement D_{x0} with $R = 60$ mm, $P = 2000$ N/m, $\eta = 0.3$ and $Q/\eta P = 0.5$, point A in Figure 3.

Figure 19 discusses the effect of the resultant electric charge Γ on the in-plane stress σ_{xx0} and the in-plane electric displacement D_{x0} for both insulating and conducting punches with $Q/\eta P = 0.5$ and $\eta = 0.3$. We can observe that the in-plane stress distribution of the insulating punch is similar to that of the conducting punch. The maximum tensile stress of the insulating punch is greater than that of the conducting punch. However, the in-plane electric displacement distribution is totally different than that of the conducting punch. The in-plane electric displacement is singular at the edge of the contact region for the conducting punch whereas it is quite smooth for the insulating punch. The change of Γ has a slight effect on both σ_{xx0} and D_{x0} .

7. Conclusions

In this paper, the two-dimensional fretting contact between a homogeneous transversely isotropic piezoelectric half-plane and a rigid conducting cylindrical punch was considered. The two dissimilar bodies are first acted upon by a monotonically increasing normal load, and then by a cyclic tangential load. The fretting contact problem is reduced to a set of coupled Cauchy singular integral equations which are solved by using an iterative method to determine the contact tractions, electric charge and unknown stick/slip region. It was found that:

- (1) The electric charge is singular at the edge of the contact region whereas the normal contact pressure and tangential traction is quite smooth.
- (2) The friction coefficient has a slight effect on the normal contact pressure and electric charge. The peak value of the tangential traction occurs at the interface between the stick region and slip region, and increases rapidly with the increase of the friction coefficient.
- (3) With the increase of the applied electric charge, the value of the tangential traction decreases at the stick region and changes slightly at the slip region.

- (4) The peak values of tangential traction for the insulating punch is greater than that of the conducting punch, but the size of the stick region is smaller than that of the conducting punch.
- (5) The maximum values of the in-plane tensile stress and the in-plane electric displacement occur at the edges of the contact region during the tangential loading phase, which implies a possible site of electromechanical damage.

Acknowledgments

The work described in this paper is supported by the Fundamental Research Funds for the Central Universities under grant number 2016YJS113.

Appendix

The parameters f_{ij} may be written in the form

$$f_{ij} = sF_{ij}, \quad i, j = 1, 2, 3, \quad (\text{A.1})$$

where

$$[F] = \begin{bmatrix} 1 & 1 & 1 \\ a_1 & a_2 & a_3 \\ b_1 & b_2 & b_3 \end{bmatrix} \begin{bmatrix} c_{13}is + c_{33}a_1n_1 + e_{33}b_1n_1 & c_{13}is + c_{33}a_2n_2 + e_{33}b_2n_2 & c_{13}is + c_{33}a_3n_3 + e_{33}b_3n_3 \\ c_{44}n_1 + c_{44}isa_1 + e_{15}isb_1 & c_{44}n_2 + c_{44}isa_2 + e_{15}isb_2 & c_{44}n_3 + c_{44}isa_3 + e_{15}isb_3 \\ e_{31}is + e_{33}a_1n_1 - \epsilon_{33}b_1n_1 & e_{31}is + e_{33}a_2n_2 - \epsilon_{33}b_2n_2 & e_{31}is + e_{33}a_3n_3 - \epsilon_{33}b_3n_3 \end{bmatrix}^{-1},$$

and $[\]^{-1}$ is the inverse matrix.

For the piezoceramic PZT-4 half-plane, the parameters f_{ij} can be written as

$$\begin{aligned} f_{11} &= -7.5241 \cdot 10^{-12}i, & f_{12} &= 1.8396 \cdot 10^{-11}, & f_{13} &= 1.7328 \cdot 10^{-2}i, \\ f_{21} &= 1.7728 \cdot 10^{-11}, & f_{22} &= 7.4241 \cdot 10^{-12}i, & f_{23} &= 2.2085 \cdot 10^{-2}, \\ f_{31} &= 2.2085 \cdot 10^{-2}, & f_{32} &= -1.7328 \cdot 10^{-2}i, & f_{33} &= -8.8307 \cdot 10^7. \end{aligned} \quad (\text{A.2})$$

References

- [Cattaneo 1938] C. Cattaneo, "Sul contatto di due corpi elastici: distribuzione locale degli sforzi", *Rend. Accad. Naz. Lincei* **27**:6 (1938), 342–348, 434–436, 474–478.
- [Chen 1999] W.-Q. Chen, "Inclined circular flat punch on a transversely isotropic piezoelectric half-space", *Arch. Appl. Mech.* **69**:7 (1999), 455–464.
- [Chen 2000] W.-Q. Chen, "On piezoelectric contact problem for a smooth punch", *Int. J. Solids Struct.* **37**:16 (2000), 2331–2340.
- [Chen and Yu 2005] Z.-R. Chen and S.-W. Yu, "Micro-scale adhesive contact of a spherical rigid punch on a piezoelectric half-space", *Compos. Sci. Technol.* **65**:9 (2005), 1372–1381.
- [Choi and Paulino 2008] H. J. Choi and G. H. Paulino, "Thermoelastic contact mechanics for a flat punch sliding over a graded coating/substrate system with frictional heat generation", *J. Mech. Phys. Solids* **56**:4 (2008), 1673–1692.
- [Ciavarella 1998a] M. Ciavarella, "The generalized Cattaneo partial slip plane contact problem, I: Theory", *Int. J. Solids Struct.* **35**:18 (1998), 2349–2362.
- [Ciavarella 1998b] M. Ciavarella, "The generalized Cattaneo partial slip plane contact problem, II: Examples", *Int. J. Solids Struct.* **35**:18 (1998), 2363–2378.

- [Ciavarella and Hills 1999] M. Ciavarella and D. A. Hills, "Brief note: some observations on oscillating tangential forces and wear in general plane contacts", *Eur. J. Mech. A-Solid* **18**:3 (may 1999), 491–497.
- [Ding et al. 2000] H.-J. Ding, P.-F. Hou, and F.-L. Guo, "The elastic and electric fields for three-dimensional contact for transversely isotropic piezoelectric materials", *Int. J. Solids Struct.* **37**:23 (2000), 3201–3229.
- [Erdogan and Gupta 1972] F. Erdogan and G. D. Gupta, "On the numerical solution of singular integral equations", *Q. Appl. Math.* **29** (1972), 525–534.
- [Fan et al. 1996] H. Fan, K.-Y. Sze, and W. Yang, "Two-dimensional contact on a piezoelectric half-space", *Int. J. Solids Struct.* **33**:9 (1996), 1305–1315.
- [Giannakopoulos and Suresh 1999] A. E. Giannakopoulos and S. Suresh, "Theory of indentation of piezoelectric materials", *Acta Mater.* **47**:7 (1999), 2153–2164.
- [Gradshteyn and Ryzhik 2000] I. S. Gradshteyn and I. M. Ryzhik (editors), *Table of integrals, series, and products*, Academic Press, New York, 2000.
- [Guo and Jin 2009] X. Guo and F. Jin, "A generalized JKR-model for two-dimensional adhesive contact of transversely isotropic piezoelectric half-space", *Int. J. Solids Struct.* **46**:20 (2009), 3607–3619.
- [Hanson et al. 1989] M. T. Hanson, L. M. Keer, and T. N. Farris, "Energy dissipation in non-Hertzian fretting contact", *Tribol. T.* **32**:2 (1989), 147–154.
- [Hills et al. 1993] D. A. Hills, D. Nowell, and A. Sackfield (editors), *Mechanics of elastic contacts*, Butterworth-Heinemann, Oxford, 1993.
- [Johnson 1985] K. L. Johnson, *Contact mechanics*, Cambridge University Press, 1985.
- [Ke et al. 2008] L.-L. Ke, J. Yang, S. Kitipornchai, and Y.-S. Wang, "Electro-mechanical frictionless contact behavior of a functionally graded piezoelectric layered half-plane under a rigid punch", *Int. J. Solids Struct.* **45**:11–12 (2008), 3313–3333.
- [Keer and Farris 1987] L. M. Keer and T. N. Farris, "Effects of finite thickness and tangential loading on development of zones of microslip in fretting", *ASLE Transactions* **30**:2 (1987), 203–210.
- [Ma et al. 2014] J. Ma, L.-L. Ke, and Y.-S. Wang, "Electro-mechanical sliding frictional contact of a piezoelectric half-plane under a rigid conducting punch", *Appl. Math. Model.* **38**:23 (2014), 5471–5489.
- [Makagon et al. 2009] A. Makagon, M. Kachanov, E. Karapetian, and S. V. Kalinin, "Piezoelectric indentation of a flat circular punch accompanied by frictional sliding and applications to scanning probe microscopy", *Int. J. Eng. Sci.* **47**:2 (2009), 221–239.
- [Mindlin and Deresiewicz 1953] R. D. Mindlin and H. Deresiewicz, "Elastic spheres in contact under varying oblique forces", *J. Appl. Mech. (ASME)* **20**:3 (1953), 327–344.
- [Mindlin et al. 1951] R. D. Mindlin, W. P. Mason, T. F. Osmer, and H. Deresiewicz, "Effects of an oscillating tangential force on the contact surfaces of elastic spheres", *J. Appl. Mech. (ASME)* **18**:3 (1951), 331.
- [Muskhelishvili 1958] N. I. Muskhelishvili, *Singular integral equations: boundary problems of functions theory and their applications to mathematical physics*, Wolters-Noordhoff Publishing, Groningen, 1958.
- [Nowell et al. 1988] D. Nowell, D. A. Hills, and A. Sackfield, "Contact of dissimilar elastic cylinders under normal and tangential loading", *J. Mech. Phys. Solids* **36**:1 (1988), 59–75.
- [Ramirez and Heyliger 2003] G. Ramirez and P. Heyliger, "Frictionless contact in a layered piezoelectric half-space", *Smart Mater. Struct.* **12**:4 (2003), 612–625.
- [Sosa and Castro 1994] H. A. Sosa and M. A. Castro, "On concentrated loads at the boundary of a piezoelectric half-plane", *J. Mech. Phys. Solids* **42**:7 (1994), 1105–1122.
- [Spence 1973] D. A. Spence, "An eigenvalue problem for elastic contact with finite friction", *Proc. Cambridge Philos. Soc.* **73**:1 (1973), 249–268.
- [Spence 1986] D. A. Spence, "Frictional contact with transverse shear", *Q. J. Mech. Appl. Math.* **39**:2 (1986), 233–253.
- [Su et al. 2015] J. Su, L.-L. Ke, and Y.-S. Wang, "Two-dimensional fretting contact analysis of piezoelectric materials", *Int. J. Solids Struct.* **73–74** (2015), 41–54.
- [Wang et al. 2008] B. B. L. Wang, J. C. Han, S. Y. Du, H. Y. Zhang, and Y. G. Sun, "Electromechanical behaviour of a finite piezoelectric layer under a flat punch", *Int. J. Solids Struct.* **45**:25–26 (2008), 6384–6398.

- [Wu et al. 2012] Y. F. Wu, H. Y. Yu, and W. Q. Chen, “Mechanics of indentation for piezoelectric thin films on elastic substrate”, *Int. J. Solids Struct.* **49**:1 (2012), 95–110.
- [Zhou and Lee 2011] Y. T. Zhou and K. Y. Lee, “Thermo-electro-mechanical contact behavior of a finite piezoelectric layer under a sliding punch with frictional heat generation”, *J. Mech. Phys. Solids* **59**:5 (2011), 1037–1061.
- [Zhou and Lee 2012] Y.-T. Zhou and K. Y. Lee, “Theory of moving contact of anisotropic piezoelectric materials via real fundamental solutions approach”, *Eur. J. Mech. — A/Solids* **35** (2012), 22–36.
- [Zhou and Lee 2014] Y.-T. Zhou and K. Y. Lee, “Investigation of frictional sliding contact problems of triangular and cylindrical punches on monoclinic piezoelectric materials”, *Mech. Mater.* **69**:1 (2014), 237–250.

Received 11 Jan 2016. Revised 10 May 2016. Accepted 16 May 2016.

JIE SU: 14115272@bjtu.edu.cn

Institute of Engineering Mechanics, Beijing Jiaotong University, Haidan District, Beijing, 100044, PR China

LIAO-LIANG KE: llke@bjtu.edu.cn

Institute of Engineering Mechanics, Beijing Jiaotong University, Haidan District, Beijing, 100044, PR China

YUE-SHENG WANG: yswang@bjtu.edu.cn

Institute of Engineering Mechanics, Beijing Jiaotong University, Haidan District, Beijing, 100044, PR China

JOURNAL OF MECHANICS OF MATERIALS AND STRUCTURES

msp.org/jomms

Founded by Charles R. Steele and Marie-Louise Steele

EDITORIAL BOARD

ADAIR R. AGUIAR	University of São Paulo at São Carlos, Brazil
KATIA BERTOLDI	Harvard University, USA
DAVIDE BIGONI	University of Trento, Italy
YIBIN FU	Keele University, UK
IWONA JASIUŁ	University of Illinois at Urbana-Champaign, USA
C. W. LIM	City University of Hong Kong
THOMAS J. PENCE	Michigan State University, USA
GIANNI ROYER-CARFAGNI	Università degli studi di Parma, Italy
DAVID STEIGMANN	University of California at Berkeley, USA
PAUL STEINMANN	Friedrich-Alexander-Universität Erlangen-Nürnberg, Germany

ADVISORY BOARD

J. P. CARTER	University of Sydney, Australia
D. H. HODGES	Georgia Institute of Technology, USA
J. HUTCHINSON	Harvard University, USA
D. PAMPLONA	Universidade Católica do Rio de Janeiro, Brazil
M. B. RUBIN	Technion, Haifa, Israel

PRODUCTION production@msp.org

SILVIO LEVY Scientific Editor

Cover photo: Wikimedia Commons

See msp.org/jomms for submission guidelines.

JoMMS (ISSN 1559-3959) at Mathematical Sciences Publishers, 798 Evans Hall #6840, c/o University of California, Berkeley, CA 94720-3840, is published in 10 issues a year. The subscription price for 2016 is US \$575/year for the electronic version, and \$735/year (+\$60, if shipping outside the US) for print and electronic. Subscriptions, requests for back issues, and changes of address should be sent to MSP.

JoMMS peer-review and production is managed by EditFlow[®] from Mathematical Sciences Publishers.

PUBLISHED BY

 **mathematical sciences publishers**
nonprofit scientific publishing

<http://msp.org/>

© 2016 Mathematical Sciences Publishers

Journal of Mechanics of Materials and Structures

Volume 11, No. 5

December 2016

- Interface stress of orthotropic materials with a nanodefekt under antiplane shear loading**
JUNHUA XIAO, CHUANFU SHI, YAOLING XU and FUCHENG ZHANG 491
- Propagation of waves in masonry-like solids**
MARIA GIRARDI, CRISTINA PADOVANI and DANIELE PELLEGRINI 505
- Two-dimensional fretting contact of piezoelectric materials under a rigid conducting cylindrical punch**
JIE SU, LIAO-LIANG KE and YUE-SHENG WANG 535
- An anisotropic model for the Mullins effect in magnetoactive rubber-like materials**
M. H. B. M. SHARIFF and ROGER BUSTAMANTE 559
- Predictive modeling of mechanical properties of metal filled anodic aluminum oxide**
VLADIMIR V. BARDUSHKIN, YULIA I. SHILYAEVA,
SERGEY A. GAVRILOV, MAXIM V. SILIBIN, VICTOR B. YAKOVLEV,
MIKHAIL L. ZHELUDKEVICH and NATALIA I. POPENKO 583
- The hemispherical nanopit at the plane boundary of an elastic half-space subjected to statically equivalent shear tractions**
CHANGWEN MI, ZHONGWEI SUN and DEMITRIS KOURIS 595
- Book review: Shorr's *Thermal integrity in mechanics and engineering***
FEODOR M. BORODICH 615



1559-3959(2016)11:5;1-4